American Mineralogist, Volume 88, pages 1033–1045, 2003

Monte Carlo simulations of ordering of Al, Fe, and Mg cations in the octahedral sheet of smectites and illites

C. IGNACIO SAINZ-DÍAZ,[1,*] ERIKA J. PALIN,[2] MARTIN T. DOVE,[2] AND ALFONSO HERNÁNDEZ-LAGUNA[1]

[1] Estación Experimental del Zaidín (CSIC), C/ Profesor Albareda, 1. 18008-Granada, Spain
[2] Department of Earth Sciences, University of Cambridge, Downing Street, Cambridge CB2 3EQ, U.K.

ABSTRACT

The ordering of Al^{3+}, Fe^{3+}, and Mg^{2+} cations along the octahedral sheet in dioctahedral 2:1 phyllosilicates was studied theoretically. The distribution of Fe^{3+}/Mg^{2+} was studied in the octahedral sheet and is compared with the Al^{3+}/Fe^{3+} and Al^{3+}/Mg^{2+} distributions. The cation exchange interaction parameters J_n, as first, second, third, and fourth nearest neighbors were calculated by means of empirical interatomic potentials. Several compositions with different interlayer cations, and tetrahedral charge close to ferric smectites, illites, and nontronites were studied. From these J_n values, a trend to form FeMg pairs was observed in the Fe/Mg system. Monte Carlo (MC) simulations based on the previously calculated cation exchange potentials J_n of these systems showed ordering phase transitions in the distribution of the octahedral cations, with different ordering patterns in each case. The two-species model was extended to a three-species ordering MC simulation model. A new procedure to study the ordering of three species is presented in this paper. We present for the first time a theoretical study of the ordering of three octahedral cations Al^{3+}, Fe^{3+}, and Mg^{2+} in clays, describing compositions more realistic for dioctahedral clay minerals, by means of Monte Carlo simulations based only on atomistic models. Short-range ordering of Fe was found in compositions of smectites and illites reproducing experimental cation distribution patterns.

INTRODUCTION

In dioctahedral 2:1 phyllosilicates, isomorphous substitution of Al^{3+} by Fe^{3+} and Mg^{2+} in the octahedral sheet and Si^{4+} by Al^{3+} in the tetrahedral sheet occurs in nature, giving a great diversity of 2:1 phyllosilicates (e.g., micas, smectites, illites, beidellites, montmorillonites, phengites, nontronites, etc.). Determination of the distribution of cations within the sheets is a complex problem, especially in the octahedral sheet, to which we refer in this paper. This type of study can be useful to understand natural processes, such as the smectite to illite transformation, dehydroxylation processes, and to analyze how cation distribution affects lattice stability. Also, the industrial and environmental applications of clays due to their valuable catalytic and adsorptive properties (e.g., as a barrier in nuclear waste and pollutant disposal repositories) make it of great interest to establish a firm theoretical understanding of their structure and behavior.

Cation distribution in aluminosilicates has been one of the important aspects of mineral behavior for a long time. Spectroscopic IR and NMR methods are especially useful for cation distribution analysis since they probe local environments and can detect short-range cation relationships. From IR studies of celadonites Besson et al. (1987) showed that octahedral cation distribution is not random and Al^{3+} and Fe^{3+} tend to segregate from each other. Drits et al. (1997) studied the isomorphous cation distribution in celadonites, glauconites, and Fe-illites by IR, Mössbauer, and EXAFS spectroscopies together with statistical analysis, and found a certain short-range ordering. In some synthetic smectites, Grauby et al. (1991) found that Al^{3+} and Fe^{3+} tend to mix rather than to segregate, Mg^{2+} and Fe^{3+} segregate within the same layer, and Mg^{2+} and Al^{3+} segregate creating dioctahedral and trioctahedral layers. Using ^{27}Al NMR to study montmorillonite, Morris et al. (1990) found that Fe was either segregated from Al in the octahedral sheet or present in a phase different from smectite. Schroeder (1993) found by means of ^{27}Al NMR that Fe mixes with Al in shale illite-smectite (I-S) samples with low Fe content but Fe segregates from Al in Fe-rich specimens. Muller et al. (1997) studied octahedral cation distribution of the Camp-Bertaux montmorillonite using XRD, EXAFS, and FTIR, and observed that Mg and Fe form clusters that segregate from Al. Therefore, these different results make it difficult to extract a definitive conclusion from all these experimental studies.

Atomistic calculations with interatomic empirical potentials can reproduce the structure and properties of aluminosilicates, particularly phyllosilicates (Sainz-Díaz et al. 2001a, 2001b; Collins and Catlow 1992), and they are used to determine ordering energies (Bosenick et al. 2000, 2001; Thayaparam et al. 1996; Palin et al. 2001). Monte Carlo (MC) simulations are a powerful tool for the study of cation distribution and ordering in minerals, especially aluminosilicates (Dove and Heine 1996; Dove et al. 1996; Warren et al. 2001). Previous studies of octahedral cation distribution (Al, Fe, and Mg) in a series of illite-smectite (I-S) mixed-layer samples using FTIR and ^{27}Al MAS

* E-mail: sainz@eez.csic.es

NMR data, and Reverse Monte Carlo (RMC) calculations, showed Fe segregation by short-range Fe ordering (Cuadros et al. 1999; Sainz-Díaz et al. 2001c). Calculations for most of the illite specimens, however, suggested medium- or long-range Fe ordering. Cation ordering in the tetrahedral sheet in muscovite was studied by means of Monte Carlo simulations, which showed long-range ordering of the tetrahedral Si and Al cations (Palin et al. 2001). Recently, Monte Carlo simulations of Al/Mg and Al/Fe cation distributions along the octahedral sheet in smectites have been showing order-disorder transitions (Sainz-Díaz et al. 2003). One of the aims of the present work is to extend this study to more realistic samples, especially with respect to the octahedral sheet composition, where Al^{3+}, Fe^{3+}, and Mg^{2+} cations co-exist simultaneously, as in the natural dioctahedral clay minerals.

METHODS

Mineral models

Models of smectites with different compositions were studied (Table 1). Two different interlayer cations were included, Na^+ and K^+, to study the effect of the interlayer cation type on the ordering in the octahedral sheet. Different tetrahedral charges were also considered to simulate the smectite [tetrahedral charge (TC) of 0.28 per unit cell] and illite (TC = 0.8 per unit cell) systems. A 2 × 2 × 1 supercell was built with periodic boundary conditions. This supercell includes 164 atoms and 16 octahedral sites. The supercell was built from a unit cell with experimental geometry (Tsipursky and Drits 1984) previously optimized by GULP allowing relaxation of the cell volume. Previous studies of micas with low tetrahedral Al contents found a non-ordered distribution of the cations in the tetrahedral sheet, which agrees with the Loewenstein rule of Al-Al pair avoidance (Herrero and Sanz 1991; Warren et al. 2001). This random distribution was included by imposing partial occupancies of Si and Al at the crystallographic positions of the tetrahedral sheet in our calculations.

Series of 90 disordered and six ordered configurations were generated for each composition using a computer program (MCclay98) described previously by Cuadros et al. (1999). For each configuration, all KL cation pairs (K = Al^{3+}, Mg^{2+}, and Fe^{3+}, and L = Al^{3+}, Mg^{2+}, and Fe^{3+}) as first, second, third, and fourth nearest neighbors were calculated, also using MCclay98 (Cuadros et al. 1999; Sainz-Díaz et al. 2001c).

Model of interatomic potentials

The basic interatomic potential model was described previously elsewhere (Sainz-Díaz et al. 2001a). These potentials are Coulomb interactions between the ionic charges and a short-range function, which describes the non-Coulombic interactions between ions, that is the Pauli repulsion at short range and the dispersion forces at longer ranges (Abbot et al. 1989a, 1989b). Electrostatic Coulomb interactions are evaluated by the Ewald method using formal charges on all atoms, except for the OH species whose component atoms have partial charges chosen so as to reproduce the dipole moment of the OH group. The overall charge on the molecular hydroxyl ion is the formal charge of –1*e*. This charge is distributed as +0.426*e* for the H atom and –1.426*e* for the O atom. This distribution is based on previous quantum mechanical calculations (Schröder et al. 1992). The intramolecular OH interaction is described by a Morse potential,

$$E = \varepsilon\left\{1 - \exp\left[-\alpha(r-\mu)\right]\right\}^2 \quad (1)$$

where r and μ are the observed and equilibrium interatomic distances, respectively. A cut-off of 1.4 Å was considered for this potential. The parameters ε, α, and μ are described in Table 2. Coulomb forces are not included between atoms coupled by a Morse potential, since it is assumed that this potential describes all components of the interactions between both atoms.

The electronic polarizability effect of all O atoms (except those in the hydroxyl groups) was modeled by means of the shell model. In this model the atoms consist of a core comprising the nucleus and tightly bound inner electrons, surrounded by a massless shell of the remaining outer electrons. The core is assigned a charge of +0.84819*e* and the shell a charge of –2.84819*e*, maintaining a formal value for the overall ionic charge of –2*e*. The shell and core are held together by an ideal harmonic core-shell interaction,

$$E = \tfrac{1}{2}(k_{sh} r_{sh}^2) \quad (2)$$

where k_{sh} is the harmonic spring constant and r_{sh} is the separation between the centers of core and shell of the O atoms.

The short-range interactions between the Si^{4+} cation and the shell of O atoms and those between shells of O atoms are described by Buckingham potentials,

$$E = A\exp(-r/\rho) - Cr^{-6} \quad (3)$$

where r is the interatomic distance, the parameters A, ρ, and C are presented in Table 2, and the exponential and the Cr^{-6} terms describe the repulsive energy and the longer range attraction, respectively. The interactions between the rest of the cations and O-atom shells are described by Born-Mayer potentials,

$$E = A\exp(-r/\rho) \quad (4)$$

The long-range interactions between H atoms and O atoms (OH···O) are described by an H-O Born-Mayer potential (Winkler et al. 1991).

An empirical Al^{3+}-O^{2-} potential was used for all coordina-

TABLE 1. Chemical composition of the systems studied and average values of the cell parameters of the structures optimized

sample	Si^{4+}	Al^{3+} (T)	Al^{3+} (O)	Mg^{2+}	Fe^{3+}	IC	*a*	*b*	*c*	β
1	7.72	0.28	3	1		$K_{1.28}$	5.22(1)	8.91(2)	10.14(5)	102.5(3)
2	7.72	0.28	3	1		$Na_{1.28}$	5.22(1)	8.91(1)	10.18(2)	105.1(3)
3	7.2	0.8	3	1		$K_{1.8}$	5.22(1)	8.93(1)	10.03(2)	102.4(2)
4	7.72	0.28	3		1	$K_{0.28}$	5.24(1)	8.90(2)	9.54(3)	96.0(2)
5	7.2	0.8	3		1	$K_{0.8}$	5.22(0)	8.93(1)	10.24(1)	102.5(1)
6	7.72	0.28		2	2	$K_{2.28}$	5.20(1)	8.96(1)	9.87(1)	101.6(1)

Note: Structural formulae on the unit-cell basis for $O_{20}(OH)_4$. Values in brackets represent the standard error in the last figure. Experimental values for similar composition are: *a* = 5.18 Å, *b* = 8.98 Å, *c* = 10.08–10.13 Å, b = 100.2–101.4° for $(Ca_{0.12}Na_{0.4}K_{0.1-0.6})(Al_{2.7-3.2}Fe^{3+}_{0.5-0.2}Mg_{1-0.2})(Si_{7-8}Al_{1-0})O_{20}(OH)_4$; *a* = 5.18 Å, *b* = 8.97 Å, *c* = 10.20 Å, β = 101.3° for $(Ca_{0.11}Na_{0.34}K_{0.14})(Al_{2.78}Fe^{3+}_{0.52}Fe^{2+}_{0.1}Mg_{0.6})Si_8O_{20}(OH)_4$; *a* = 5.20 Å, *b* = 9.01 Å, *c* = 10.20 Å, β = 101.3° for $(Ca_{0.22}Na_{0.06}K_{0.32})(Al_{1.92}Fe^{3+}_{1.76}Mg_{0.52})(Si_{7.06}Al_{0.94})O_{20}(OH)_4$ (Tsipursky and Drits 1984). T = tetrahedral, O = octahedral, IC = interlayer cation.

TABLE 2. Parameters of the interatomic potential models used in this work

Interatomic interaction	Parameters		
Shell-core interaction*	k_{sh} (eV Å^{-2})	q_{core}	q_{shell}
O_{core}-O_{shell}	74.92	+0.86902	−2.86902
Buckingham potentials*†	A (eV)	ρ (Å)	C (eV Å^{-6})
$(O^{2-})_{shell}$-$(O^{2-})_{shell}$	22764.0	0.149	27.88
Si^{4+}-$(O^{2-})_{shell}$	1283.9073	0.3205	10.6616
Born-Mayer potentials†	A (eV)	ρ (Å)	
$[Si^{4+}$-$(O^{1.426-})_{core}]$*	999.98	0.3012	
$[Al^{3+}$-$(O^{1.426-})_{core}]$‡	1142.6775	0.2991	
$[Al^{3+}$-$(O^{2-})_{shell}]$*	1460.3	0.2991	
$[Fe^{3+}$-$(O^{2-})_{shell}]$§	3219.335	0.2641	
$[Fe^{3+}$-$(O^{1.426-})_{core}]$§	3219.335	0.2641	
$[Mg^{2+}$-$(O^{1.426-})_{core}]$*	1142.6775	0.2945	
$[Mg^{2+}$-$(O^{2-})_{shell}]$*	1428.5	0.2945	
$[K^{+}$-$(O^{2-})_{shell}]$*	65269.71	0.2130	
$[Na^{+}$-$(O^{2-})_{shell}]$§	1271.504	0.3000	
$[(H^{0.426+})_{core}$-$(O^{2-})_{shell}]$*	325.0	0.25	
Morse potential*	ε (eV)	α (Å^{-1})	μ (Å)
$(H^{0.426+})_{core}$-$(O^{1.426-})_{core}$	7.0525	2.1986	0.9485
Three-body bond-bendingǁ	k (eVrad^{-2})	θ_0 (°)	
$[O^{2-}$-T-$O^{2-}]$*	2.09724	109.47	
$[O^{2-}$-M-$O^{2-}]$*	2.09724	90	
O^{2-}-M-$O^{1.426-}$	2.09724	90	
$O^{1.426-}$-M-$O^{1.426-}$	2.09724	90	

* From Winkler et al. (1991).
† Cut-off at 12 Å.
‡ From Schröder et al. (1992).
§ From Bush et al. 1994.
ǁ T = cation in the tetrahedral sheet (Si^{4+} or Al^{3+}), M = any cation in the octahedral sheet (Al^{3+}, Fe^{3+}, or Mg^{2+}).

tions (Jackson and Catlow 1988). Although the OH groups are joined to cations of the octahedral sheet, they are close to the cations of the tetrahedral sheet, therefore we included an empirical $Si^{4+}{}_{core}$-$O^{1.426-}{}_{core}$ potential for the Si/OH interactions (Collins and Catlow 1992). Since the isomorphous substitution of Mg and Fe occur in the octahedral sheet, the Mg-O and Fe-O potentials were also included for both types of O atoms ($O^{2-}{}_{shell}$ and $O^{1.426-}{}_{core}$). For modeling the interlayer space interactions with exchange cations, the K-O potential from Post and Burnham (1986) and Na-O potential from Bush et al. (1994) described quite well the interlayer interactions.

Covalent effects are simulated using three-body bond-bending interactions,

$$E = 1/2k(\theta - \theta_0)^2 \quad (5)$$

where k is the harmonic three-body force constant, and θ and θ_0 are the observed and ideal bond angles, respectively. The parameters k and θ_0 (Table 2) are identical for all atoms within the same coordination.

This shell model with these interatomic potentials and all these parameters have been used to model accurately structures and crystal properties of the main rock-forming silicate minerals (Bosenick et al. 2000, 2001; Dove and Heine 1996; Dove et al. 1996; Thayaparam et al. 1996) and layer 2:1 phyllosilicates (Collins and Catlow 1992; Palin et al. 2001), particularly smectites and illites (Sainz-Díaz et al. 2001a, 2001b), with a high level of transferability. All lattice energy calculations were performed with the GULP code with the Newton-Raphson minimization method for the lattice relaxation (Gale 1997).

Simulations of cation ordering

For the cation ordering simulations we first compute the ordering interactions by means of interatomic potentials and lattice energy relaxation methods, and then use Monte Carlo methods to simulate the ordering process as a function of temperature (Bosenick et al. 2001; Warren et al. 2001).

The energy related with the ordering interactions can be extracted from the above lattice energy calculations of these configurations. This approach makes use of a model Hamiltonian for the ordering interactions. Taking into account separate pair interactions for two ordering cations, the energy of each configuration can be expressed as

$$H = E_0 + \sum_n (N^n_{M-M}E^n_{M-M} + N^n_{M'-M'}E^n_{M'-M'} + N^n_{M-M'}E^n_{M-M'}) \quad (6)$$

where n indicates different types of neighboring pairs of cations, N is the number of cation pairs for each type, E is the partial energy related with this cation pairing, and M and M' are different octahedral cations (Al^{3+}, Mg^{2+}, or Fe^{3+}). The total energy requires summation over all types of interactions. E_0 indicates all other components of bond energies and any energy that has no effect on the ordering process, and hence is a constant for our ordering study. The energy terms for each neighbor pair can be combined into a single parameter called the exchange parameter (J). This parameter indicates the energy associated with the exchange of two cations to form M–M and M'-M' linkages instead of two M-M' linkages. This energy expression can be reduced to

$$H = E_0 + \sum_n N^n_{M-M}(E^n_{M-M} + E^n_{M'-M'} - 2E^n_{M-M'}) \quad (7)$$

This equation can be used for the determination of the exchange interactions J with the equation:

$$H = E_0 + \sum_n N^n_{M-M}J_n \quad (8)$$

It is useful to define an ordering variable (σ) in each site for the statistical analysis of the energies. We use the value σ = –1 if the site is occupied by M and σ = +1 if the site is occupied by M' (different from M). Then, the energy can be described by the following Hamiltonian model:

$$H = E_0 + \sum_{<ij>} \sigma_i\sigma_j J_n \quad (9)$$

where <ij> shows that the sum is over all relevant pairs of octahedral sites, avoiding counting any pair twice. The Hamiltonian model holds for all values of the Al:Mg, Al:Fe, and Fe:Mg ratios of the octahedral sheet.

Ordering of three cations

For the case of three ordering cations (Al, Fe, and Mg) instead of two, the Hamiltonian model for the ordering interactions can be expressed as

$$H = E_0 + \sum_n (N^n_{AlAl}E^n_{AlAl} + N^n_{FeFe}E^n_{FeFe} + N^n_{MgMg}E^n_{MgMg} + N^n_{AlFe}E^n_{AlFe} + N^n_{AlMg}E^n_{AlMg} + N^n_{FeMg}E^n_{FeMg}) \quad (10)$$

where n represents the different types of cation neighbors of cations considered, and N indicates the number of cation pairs for each type (as in Eq. 6). A more detailed discussion of this Hamiltonian model has been reported elsewhere (Bosenick et al. 2001). The energy terms for each type of neighbor pair can be expressed in terms of the three variables N_{AlAl}, N_{FeFe}, and N_{MgMg}, as

$$\begin{aligned} H = E_0 + \sum_n N^n_{AlAl}(E^n_{AlAl} + E^n_{FeMg} - E^n_{AlFe} - E^n_{AlMg}) + \\ N^n_{FeFe}(E^n_{FeFe} + E^n_{AlMg} - E^n_{AlFe} - E^n_{FeMg}) + \\ N^n_{MgMg}(E^n_{MgMg} + E^n_{AlFe} - E^n_{AlMg} - E^n_{FeMg}) \end{aligned} \quad (11)$$

Like in Equation 8, this Hamiltonian can be expressed in terms of exchange interactions J as

$$H = E_0 + \sum_n (N^n_{AlAl}J^n_{AlAl} + N^n_{FeFe}J^n_{FeFe} + N^n_{MgMg}J^n_{MgMg}) \quad (12)$$

In this case, we have three times as many exchange constants to determine as in the case where there are only two ordering cations. This can make for a more complicated fitting procedure in the generation of exchange interactions. From Equation 12, the three exchange interactions will be for each type of neighborhood:

$$\begin{aligned} J_{AlAl} &= E_{AlAl} + E_{FeMg} - E_{AlFe} - E_{AlMg} \\ J_{FeFe} &= E_{FeFe} + E_{AlMg} - E_{AlFe} - E_{FeMg} \\ J_{MgMg} &= E_{MgMg} + E_{AlFe} - E_{AlMg} - E_{FeMg} \end{aligned} \quad (13)$$

Some help can be obtained by performing the analysis with configurations containing only two types of atoms, which can give the two-atom exchange interactions (now specifically labeled by the superscript denoting the pairs of cations for clarity):

$$\begin{aligned} J^{(AlFe)} &= E_{AlAl} + E_{FeFe} - 2E_{AlFe} \\ J^{(AlMg)} &= E_{AlAl} + E_{MgMg} - 2E_{AlMg} \\ J^{(FeMg)} &= E_{FeFe} + E_{MgMg} - 2E_{FeMg} \end{aligned} \quad (14)$$

We noted earlier that because of the constraints linking the numbers of pairs of atoms it is not possible to extract separate values of the bond energies (such as E_{AlAl} and E_{AlFe}). However, the two-atom exchange interactions provide useful constraints. By forming appropriate combinations of the two-atom exchange constants, we have

$$\begin{aligned} J^{(AlFe)} + J^{(AlMg)} - J^{(FeMg)} &= 2E_{AlAl} + 2E_{FeMg} - 2E_{AlFe} - 2E_{AlMg} = 2J_{AlAl} \\ J^{(AlFe)} + J^{(FeMg)} - J^{(AlMg)} &= 2E_{FeFe} + 2E_{AlMg} - 2E_{AlFe} - 2E_{FeMg} = 2J_{FeFe} \\ J^{(AlMg)} + J^{(FeMg)} - J^{(AlFe)} &= 2E_{MgMg} + 2E_{AlFe} - 2E_{AlMg} - 2E_{FeMg} = 2J_{MgMg} \end{aligned} \quad (15)$$

If an appropriate set of two-atom configurations is combined with the set of three-atom configurations, the database of configuration energies may be sufficiently constrained to enable the fitting procedure to be stable even with many different types of interaction. Of course, this relies on there being no non-analytic dependence of the exchange interactions on chemical composition.

Determination of exchange interactions

Different relative positions can be defined between the different octahedral sites of these configurations, according to the shortest interatomic distances in the crystal. Considering a two-dimensional plane of octahedral cations, the relative positions can be established as first, second, third, and fourth nearest neighbors if the interatomic distances are < 3.3, 5.1–5.3, 5.8–6.2, and 7.7–8.2 Å, respectively. Topologically the fourth nearest neighbor would really be an extracyclic third neighbor, but the high value of the intercationic distance makes it valid to name them as fourth neighbors (Fig. 1). Our approach is to produce a large number of configurations with different arrangements of atoms and to compute the energies of each configuration following the minimization of the lattice energy. Each configuration consists of a large unit cell that is a $2 \times 2 \times 1$ supercell of the unit cell of the system, and the periodic boundary conditions (PBC) are retained to avoid effects of surfaces and finite sizes. This cell size and the PBC allow calculation of the exchange interactions defined above between all sites and cations. Different cations are distributed across the cation sites at random. The lattice energy of each configuration is relaxed to relieve stresses associated with the exchange of cations of different sizes optimizing simultaneously all atomic positions and the crystal lattice. After the energies of many configurations have been obtained, the values of the parameters J are fitted against the database of energies. We have found that between 50–100 configurations are useful for this procedure.

All configurations optimized should be checked in terms of geometry (cell parameters, a, b, c, and β) and optimization process (final gradient normalized). In some systems, a few configurations yielded a non-minimum energy structure. In these cases, the systems were re-optimized and, if the error persisted, they were rejected. We explored so many configurations that the rejection of only a few samples did not affect the final result. In our systems, the energy minimization of the different configurations generated provided 90 different lattice energies,

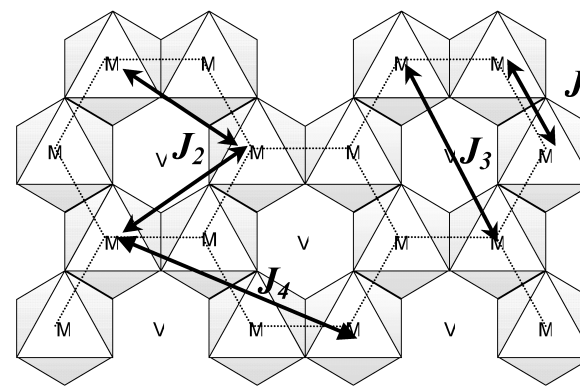

FIGURE 1. Definition of the exchange interactions between cation neighbors within an octahedral layer in a $2 \times 2 \times 1$ supercell.

which formed a set of values for E in the Equation 8. These energies and the number of Al–Al interactions for each exchange pair for each configuration calculated by our program generated 90 equations of the form of Equation 8 with the values of E_0 and exchange interactions determined by multiple regression analysis.

Monte Carlo simulation

The Monte Carlo (MC) method was used for statistical analysis of the Hamiltonian of Equation 8. We used the Ossia code (Warren et al. 2001) that was written for use on large parallel computers, with the intention of performing parallel simulations of many different temperatures.

The MC simulation program yields information about the topology of the bonds between sites. The configuration is defined in terms of a lattice of unit cells, as in a crystal. Each unit cell contains a set of labeled cation sites. Periodic boundary conditions are applied to the simulation cell. Each configuration is defined by the set of cation pairs as first, second, third, and fourth neighbors and by the energy (H) of the Hamiltonian of Equation 8. Supercells of $16 \times 16 \times 1$ and $18 \times 18 \times 1$ were used for the two-species and three-species simulations, respectively. The starting configuration for the MC simulation can be random or can have an ordered distribution. In this configuration, two cations are selected randomly and their positions are exchanged if this action lowers the H value. If H increases the cation positions are exchanged with a probability $\exp(-H/T)$, where T is not an absolute temperature but a relative value of temperature. This step is repeated 10^6–10^8 times. In the beginning, H decreases until the system reaches equilibrium. Then, H oscillates slightly around the minimum value and all data and average values are taken at this time. This procedure was repeated at many different T values (typically between 20 and 60) following a warming or a cooling process to avoid false minimum states in the annealing simulation process.

The MC experiments yielded some expected values, including $\langle E \rangle$ and $\langle E \rangle^2$ for the energy, from which one can form the heat capacity C:

$$C = \frac{\langle E^2 \rangle - \langle E \rangle^2}{k_B T^2} \quad (16)$$

The temperature of transition (T_c) values are included in the data analysis for a better description of the phase transition. T_c for a particular system is dependent on the J values for that system, and the large variation between J values for different systems explains the corresponding variation in T_c.

The Cerius^{2} crystal visualizer program was used for monitoring the configurations produced by the MC simulations. This enabled the identification of ordered configurations, and in particular identified cases where ordering was accompanied by the formation of domain microstructures.

Results and Discussion

Ordering energy

To study the cation ordering of systems with three species (Al^{3+}, Fe^{3+}, and Mg^{2+}), different systems with two species should be studied first. Samples with octahedral compositions of Al/Mg = Al/Fe = 3/1 were studied previously (Sainz-Díaz et al. 2003) and they are included in Table 1 for comparison. For the Fe/Mg ordering study, a new sample with an octahedral composition of Fe/Mg = 1/1 was included in this work (Table 2). Although this last composition is difficult to find in natural clay samples, its study can be very useful to the ordering study of samples with three cations (Al^{3+}, Fe^{3+}, and Mg^{2+}), that correspond more closely to a real cation octahedral composition of clay minerals.

In the supercells of this work, the octahedral sites have real occupancies of cations. These $2 \times 2 \times 1$ supercells (164 and 168 atoms per supercell) were fully optimized allowing us to simultaneously optimize the atom positions and cell parameters. These optimized supercells yielded lattice parameters similar to the experimental values. In sample 4, the calculated parameters c and β are smaller than the experimental ones. In this sample the interlayer charge is too small and the interlayer interactions are too weak to be described by the method of empirical potentials used in this work. Sample 6 yielded a crystal lattice with cell parameters consistent with standard experimental data for clays. In general, the small differences between calculated and experimental cell parameters can be justified by the differences in the chemical compositions between our models and experimental samples.

The different configurations of octahedral cations calculated for each model presented similar lattice parameters, with low standard deviations for each parameter value (Table 2). In general, increasing interlayer charge results in decreasing of calculated c, according to previous studies (Sainz-Díaz et al. 2001a). An increase of the interlayer charge reinforces the interactions in the interlayer space which decreases the interlayer space (Fig. 2). In our calculations we found a linear relationship in this phenomenon and this effect can be expressed quantitatively as

$$c = 10.4 – 0.246\ Q_{int}\ (R^2 = 0.9857) \quad (17)$$

where c is in Å, and Q_{int} indicates the interlayer charge per unit cell.

All configurations calculated in each sample were fitted to the Hamiltonian model of Equation 8, producing different exchange interactions (J_n, Table 3). Previous work showed that a maximum distance of 7.5–8 Å should be considered for these interactions (Sainz-Díaz et al. 2001c). Good quality fits were obtained yielding low standard errors in the values for E_0 and

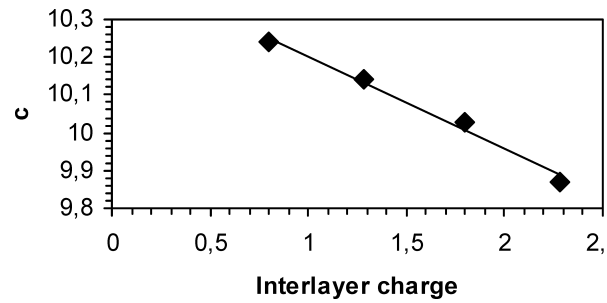

Figure 2. Relationship between the interlayer charge (per unit cell) and the parameter c (in Å).

TABLE 3. Exchange interactions (J_n) and E_0 parameter of the Hamiltonian model (in eV, values in brackets represent the standard error in the last figure)

Parameter	E_0	J_1	J_2	J_3	J_4
Distance (Å)	–	<3.3	5.1–5.3	5.8–6.2	7.7–8.2
model 1 (AlMg)	–5300.45 (66)	0.656 (16)	0.168 (14)	0.089 (18)	0.025 (8)
model 2 (AlMg)	–5299.42 (61)	0.652 (14)	0.162 (10)	0.088 (10)	0.015 (9)
model 3 (AlMg)	–5222.25 (71)	0.620 (18)	0.151 (11)	0.066 (12)	0.030 (9)
model 4 (AlFe)	–5376.14 (8)	0.025 (2)	0.007 (1)	0.003 (1)	0.003 (1)
model 5 (AlFe)	–5292.83 (15)	0.015 (3)	0.005 (2)	0.008 (3)	0.001 (2)
model 6 (FeMg)	–5211.68 (57)	0.456 (31)	0.101 (23)	–0.003 (27)	0.075 (20)

J_n. In some cases, the errors are relatively large due to correlation effects but these errors do not imply that the values are statistically insignificant. The exchange interaction parameters of samples 1–5 were recently reported (Sainz-Díaz et al. 2003) and they are included in Table 3 for comparison. The exchange parameters J_n of sample 6 have an acceptable but higher standard deviation than in other samples, probably due to the peculiar and non-natural composition and the low number of configurations calculated (50 instead of 90). Samples 1 and 2 are identical except for the substitution of K by Na as interlayer cation. Both samples present very similar exchange interaction parameters. Hence, the exchange of Na^+ by K^+ has no significant effect on the exchange interactions and consequently on the ordering of octahedral cations. Analogously, the tetrahedral charge variation did not produce significant changes in the exchange interaction values (J_n), since models 1–3 have similar values of J_n. The high and positive values of J_1 indicate that AlAl and MgMg are likely dispersed. The Al/Fe samples with different tetrahedral and interlayer charge (4 and 5) gave J_n values significantly lower than those in the Al/Mg system, indicating no significant ordering preference. In the Fe/Mg model (model 6), the J_n values are significantly higher than in the Al/Fe models but lower than in the Al/Mg models, especially J_1 and J_2. This indicates a mixing preference between the Fe and Mg cations. Of note is the low and negative value of J_3 in the Fe/Mg model with respect to the rest of the systems. This shows that the relative position of two identical cations (FeFe and MgMg) most favored is as third neighbors.

MC simulations of the two-species systems

In our previous paper (Sainz-Díaz et al. 2003) we reported simulations of two-species systems corresponding to illite and smectite compositions, including simulations of Al/Mg 1/1 and 3/1 compositions, and the Al/Fe 3/1 composition. The Al/Mg 1/1 composition gave ordering with different species in nearest-neighbor sites, as expected from the values of the exchange interactions, with a transition temperature of 1600 K.

The two 3/1 systems gave different ordered structures, reflecting subtle differences in the balance of the values of exchange interactions for different neighbors. In the Al/Mg 3/1 system, the most stable configuration was an ordered distribution where the Mg atoms are maximally dispersed, with an ordering temperature of 300 K. This Al/Mg ordering is similar for smectites and illites, that is, for different tetrahedral charge or interlayer cations. This result is consistent with experimental results for dioctahedral smectites and illites, where no MgMg pair is detected (Cuadros et al. 1999). In addition, FTIR and ^{27}Al NMR data together with RMC simulations validate these theoretical simulations indicating also the highly dispersed distribution of Mg^{2+} in the octahedral sheet (Sainz-Díaz et al. 2001c). The Al/Fe 3/1 system gave a phase transition at a much lower temperature (30 K). This ordered configuration has all Fe^{3+} cations highly dispersed within the octahedral sheet, according to the experimentally observed mixing tendency of Al and Fe cations in synthetic smectites (Decarreau et al. 1992; Grauby et al. 1991). In natural shale illite-smectite samples with low Fe contents, Schroeder (1993) also found that Fe mixes with Al in the octahedral sheet.

To help appreciate the effects of the values of the exchange interactions, we also performed MC simulations on the Al/Fe (using the J values from models 4 and 5) and Fe/Mg (using the set of J_n from model 6) 1/1 systems, giving a comparison with the previous Al/Mg 1/1 system. Both systems show evidence for phase transitions, as can be seen from the heat capacity graphs in Figure 3. From these data we see that the phase transition in the Al/Fe system occurs at a significantly lower temperature, 90 K in model 4 and 75 K in model 5, than in both the Al/Mg system (described above) and the Fe/Mg 1/1 system (2000 K). Figures 4 and 5 show snapshot configurations from the MC experiments for both the Al/Fe and Fe/Mg 1/1 simulations, respectively, showing disordered, partially ordered with domain walls, and completely ordered arrangements of atoms. The ordering is of the same type in all three systems, where the cations are completely mixed. No homo-cationic pairs (AlAl, FeFe, or MgMg) were found and the configuration is controlled only by J_2 interactions.

In the Al/Fe systems, all Fe^{3+} cations are highly dispersed, although the ordering phase transition occurs at much lower temperature than in other systems. This could mean that the dispersion tendency of Fe^{3+} is much lower than that of Mg^{2+} in these systems. However, in many natural dioctahedral clays with Al^{3+}, Fe^{3+}, and Mg^{2+} cations in the octahedral sheet, and a high Fe content, the segregation tendency of Fe was observed experimentally (Morris et al. 1990; Cuadros et al. 1999; Sainz-Díaz et al. 2001c). This disagreement with our previous MC simulations can be explained by the fact that the presence of Mg in the octahedral sheet probably helps Fe^{3+} segregate. This hypothesis is based on the values of J_n that are considerably higher in Al/Mg and Fe/Mg systems than in Al/Fe systems, especially J_1 and J_2. Therefore, a three-species ordering study should be performed to understand the cation distribution behavior.

MC simulations of three-species systems

Different Al/Fe/Mg compositions were used for the MC simulations to observe the effect of this octahedral sheet composition in the cation ordering. The initial composition Al/Fe/

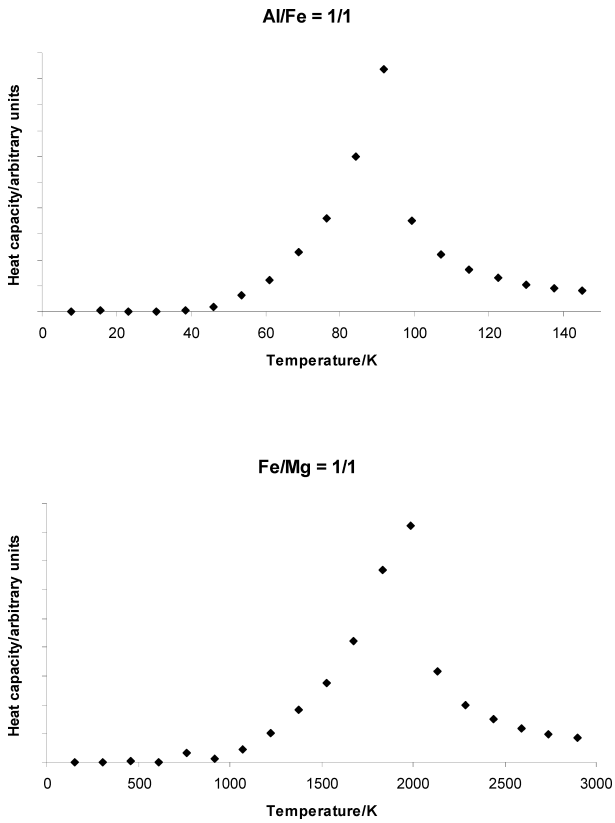

FIGURE 3. MC results for the temperature dependence of the heat capacity for simulations of the octahedral cation distribution for Al/Fe = 1/1 (model 4) and Fe/Mg = 1/1 (model 6).

Mg = 1/1/1 is used as a standard model with the same relative proportion for all cations. The Al/Fe/Mg = 1/3/2 model can represent a nontronite with a high content of Mg^{2+}. The Al/Fe/Mg = 3/2/1 model can represent a ferric smectite. The Al/Fe/Mg = 4/1/1 model is representative of the octahedral sheet of most common smectites and illites. Therefore, the three-species models let us work with more realistic systems.

Exchange interactions. We derived values for interactions for the tri-cation systems using the two-atom exchange interactions in Table 3 and Equation 15. These are given in Table 4 as different series of values: (1) Averaged values, derived from averaged values of the two-atom exchange interactions (averaged values from samples 1–3 for the Al/Mg systems, averaged values from samples 4 and 5 for the Al/Fe systems, and values from 6 for the Fe/Mg mixture). This is reasonable since the MC simulations for two species gave similar behavior for samples 1–3, and samples 4 and 5 showed similar behavior in the Al/Fe 1/1 system; (2) Smectitic series, that are values derived from the two-atom exchange interactions of samples with low interlayer charge, like samples 1 and 4; and (3) Illitic series, derived from samples with higher interlayer charge, like samples 3 and 5. Data from sample 6 were used in all series of two-atom exchange interactions (Table 4).

Most of these three-cation samples show evidence for ordering phase transitions, as can be seen from the heat capacity graphs in Figure 6. Additionally, these ordering phase transitions can usually be observed clearly by plotting the evolution of a number of $J_{n,i-i}$ (i = Al, Fe, and Mg) with temperature, which shows drastic changes of $nJ_{n,i-i}$ at the phase transition temperature (see below).

Al/Fe/Mg:1/1/1. The Al/Fe/Mg:1/1/1 system shows an ordering phase transition from the heat capacity profile (Fig. 6) and the $nJ_{n,i-i}$ plots (Fig. 7). This model is especially interesting, due to the novel ordered superstructure that can be seen. A snapshot of the structure at low temperature is shown in Figure 8. The ordered structure has rings of Fe atoms joined by J_1 interactions, surrounded by larger rings of Al joined by J_1, J_2, and J_4 interactions and Mg joined by J_2, J_3 and J_4 interactions. The configuration in Figure 8 shows only a few ordering defects; for example, some Al atoms can be seen within what one would expect to be the sixfold rings of J_1-linked Fe atoms. Partial ordering patterns for each cation are presented in Figures 8b-8d, in which similar cations are joined through J_2 and J_3 links for Mg (Fig. 8b), J_1 links for Fe (figure 8c), and J_1 and J_2 links for Al (figure 8d). The long-range ordering is perfect for the Mg cations (Fig. 8b) and near-perfect for the Al (Fig. 8d)

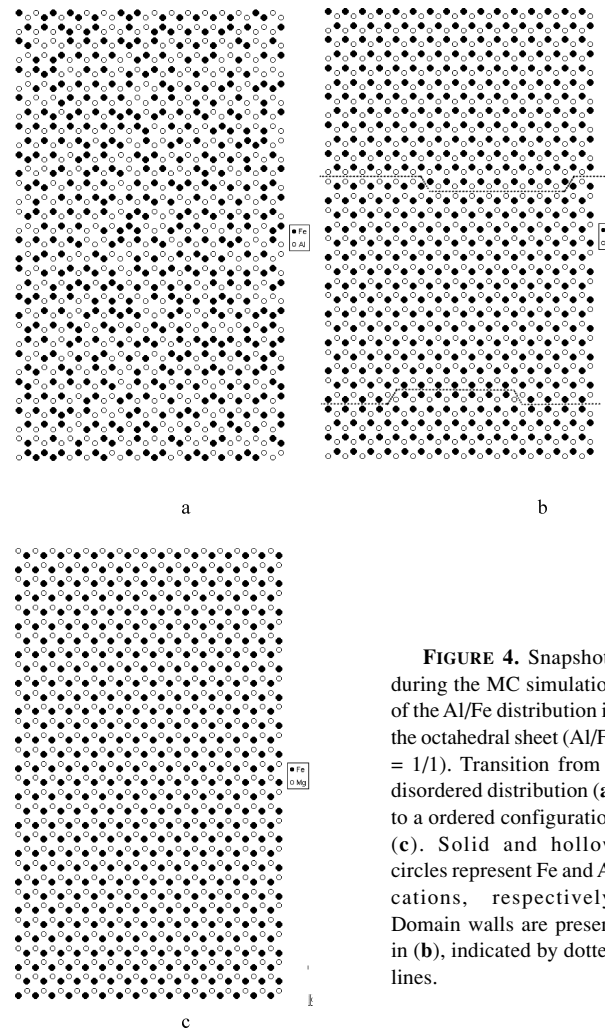

FIGURE 4. Snapshots during the MC simulation of the Al/Fe distribution in the octahedral sheet (Al/Fe = 1/1). Transition from a disordered distribution (**a**) to a ordered configuration (**c**). Solid and hollow circles represent Fe and Al cations, respectively. Domain walls are present in (**b**), indicated by dotted lines.

and Fe (Fig. 8c) cations with only a few ordering defects.

One significant aspect of the ordered Al/Fe/Mg: 1/1/1 model is that there are no MgMg nearest-neighbor pairs. This is consistent with the experimental behavior of Mg^{2+} in the octahedral sheet of smectites, illites (Sainz-Díaz et al. 2001c), and nontronites (Manceau et al. 2000). On the other hand, in the MC simulations the Fe^{3+} cations segregate in small globular clusters, according to experimental results that found a segregation tendency of Fe^{3+} in natural smectites and illites from IR, NMR spectroscopy, and RMC simulations (Sainz-Díaz et al. 2001c). Manceau et al. (2000) also found small Fe domains separated by Al and Mg cations in nontronites and this is consistent with the lack of magnetic ordering observed in these minerals at low temperatures (Lear and Stucki 1990).

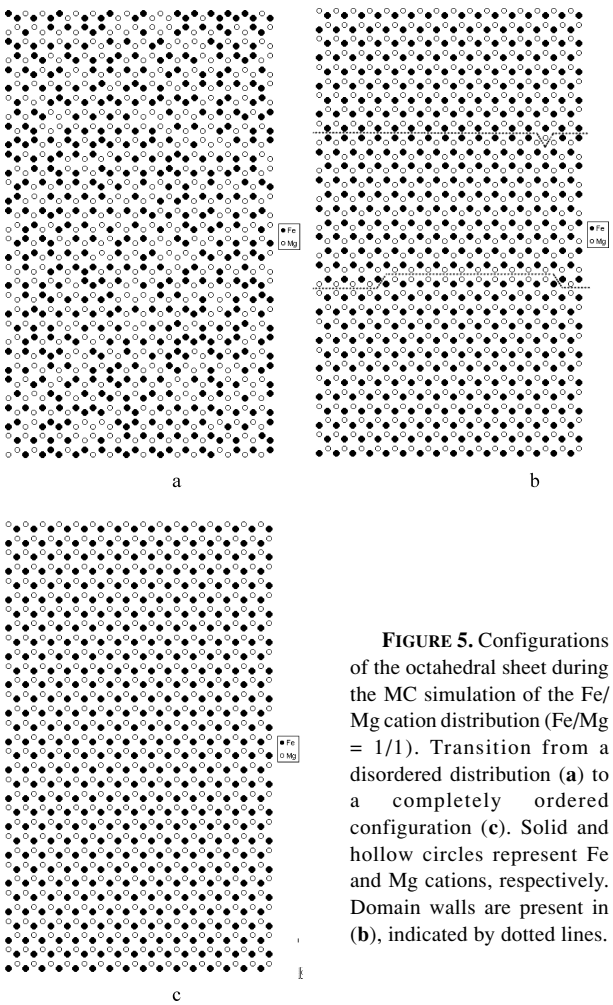

FIGURE 5. Configurations of the octahedral sheet during the MC simulation of the Fe/Mg cation distribution (Fe/Mg = 1/1). Transition from a disordered distribution (**a**) to a completely ordered configuration (**c**). Solid and hollow circles represent Fe and Mg cations, respectively. Domain walls are present in (**b**), indicated by dotted lines.

Al/Fe/Mg:1/3/2. The Al/Fe/Mg:1/3/2 system appears to show ordering behavior in the heat capacity data (Fig. 6), but the snapshot configuration at low temperature given in Figure 9 shows a complex behavior. It appears that there is a segregation into different ordered structures. Parts of the structure show an attempt at ordering in the Al/Fe/Mg = 1/1/1 pattern, and at the bottom right, there is a region of Fe/Mg 3/1 forming a "superhexagon" pattern. There are also small regions of Al/Mg 1/1 and Fe/Mg 1/1. This ordering can be observed more easily in the partial ordering patterns for each cation, where the existence of different ordering domains can be detected, in particular for Mg (Fig. 9b) and Fe (Fig. 9c) cations. A rather lower degree of long-range ordering is observed for the Al cations (Fig. 9d).

In this mixture of ordering patterns, no MgMg pair is detected, and the Mg cations are dispersed with J_2, J_3, and J_4 MgMg interactions. On the contrary, Fe^{3+} tends to segregate in small clusters.

Although this octahedral composition is not very common in nontronites due to the high Mg content, we can compare it with experimental data from nontronites due to the high Fe content. Thus, the results of this MC simulation are consistent with experimental order-disorder studies on nontronites, where no long-range order was detected, although the same tendency toward local ordering was reported (Manceau et al. 2000).

Al/Fe/Mg:3/2/1. MC simulations of the Al/Fe/Mg:3/2/1 system also showed a phase transition (Fig. 6). The ordered distribution shows attempted ordering with Fe atoms forming chains, and Al and Mg atoms segregating from Fe into different chains (Fig. 10). Perfect order was not attained in this system on the simulation length of our simulations. This fact can be observed in the partial ordering patterns (Figs. 10b–10d). The Mg^{2+} cations are very dispersed in a MgMg network dominated by J_3 interactions with a small proportion of J_2 interactions. Similar Mg arrangements were found experimentally in smectites (Sainz-Díaz et al. 2001c) and nontronites (Manceau et al. 2000). No specific ordering was found for Al^{3+} cations. The AlAl network is controlled mainly by J_1 and J_2 interactions. The Fe^{3+} cations segregate forming chain networks controlled mainly by J_1 and J_2 interactions. No crosslinking and no interchain connection was observed in the Fe chains. This segregation tendency of Fe^{3+} was also observed experimentally in natural smectites (Sainz-Díaz et al. 2001c). However, this calculated long-range order was not observed in natural samples, but only short and medium-length chains of Fe^{3+} were detected. This fact can be explained from the point of view of the natural formation process, in which the crystallization process could be too fast to yield a thermodynamically stable cation configuration.

TABLE 4. Exchange interactions for three-species systems (in eV), derived from those obtained for two-species systems (Table 3) *

Parameter	J_1	J_2	J_3	J_4
Al-Al	0.090†, 0.113‡ (0.105)	0.028†, 0.037‡ (0.033)	0.039†, 0.048‡ (0.049)	–0.022†, –0.024‡ (–0.029)
Fe-Fe	–0.075†, –0.088‡ (–0.085)	–0.023†, –0.030‡ (–0.027)	–0.031†, –0.045‡ (–0.044)	0.023†, 0.027‡ (0.031)
Mg-Mg	0.531†, 0.544‡ (0.545)	0.124†, 0.131‡ (0.127)	0.028†, 0.042‡ (0.041)	0.052†, 0.049‡ (0.049)

* Values in eV, the values in brackets are from averaged J values of two-species systems: Al/Mg values from samples 1–3, Al/Fe values from 4 and 5, and Fe/Mg values from 6.
† Values from illitic samples (3, 5, and 6).
‡ Values from smectitic samples (1, 4, and 6).

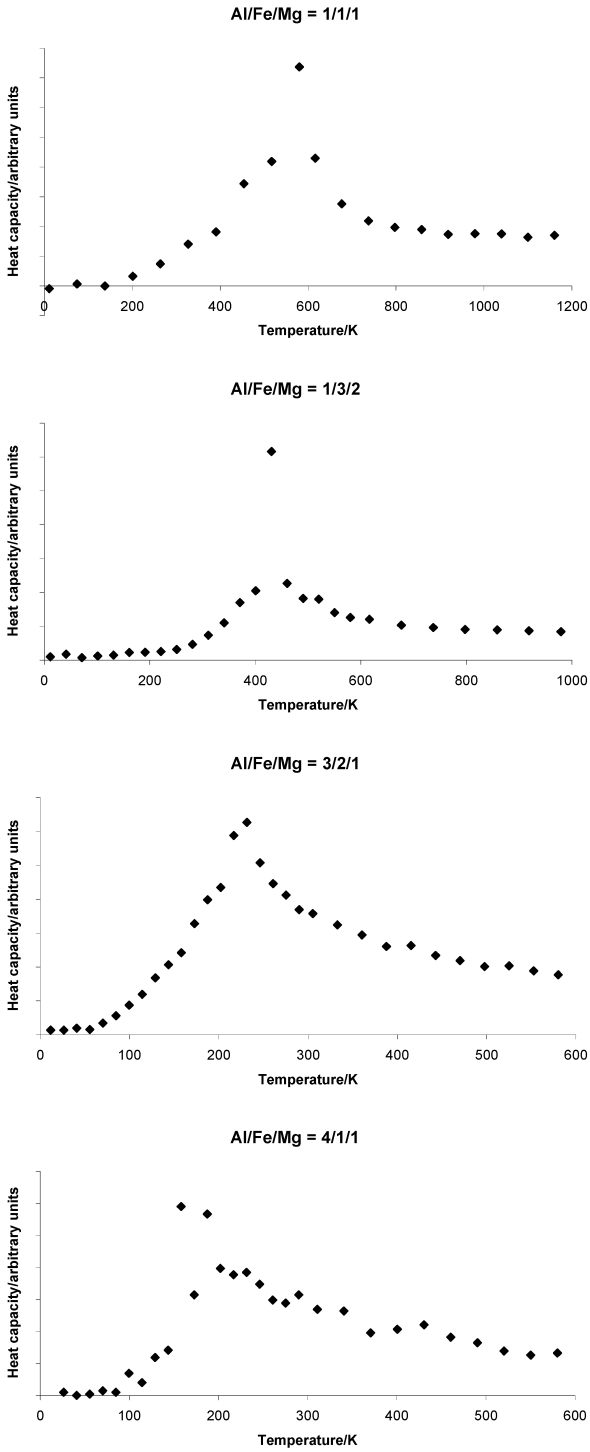

FIGURE 6. Heat capacity as a function of temperature for three-species systems with several Al/Fe/Mg ratios.

An equilibration process of cation arrangements can probably occur by means of a solid state reaction but the kinetics of this process is too slow to allow the formation of the theoretical long-range ordering.

Al/Fe/Mg:4/1/1. The 4/1/1 system represents the most common octahedral sheet composition found in natural illites and

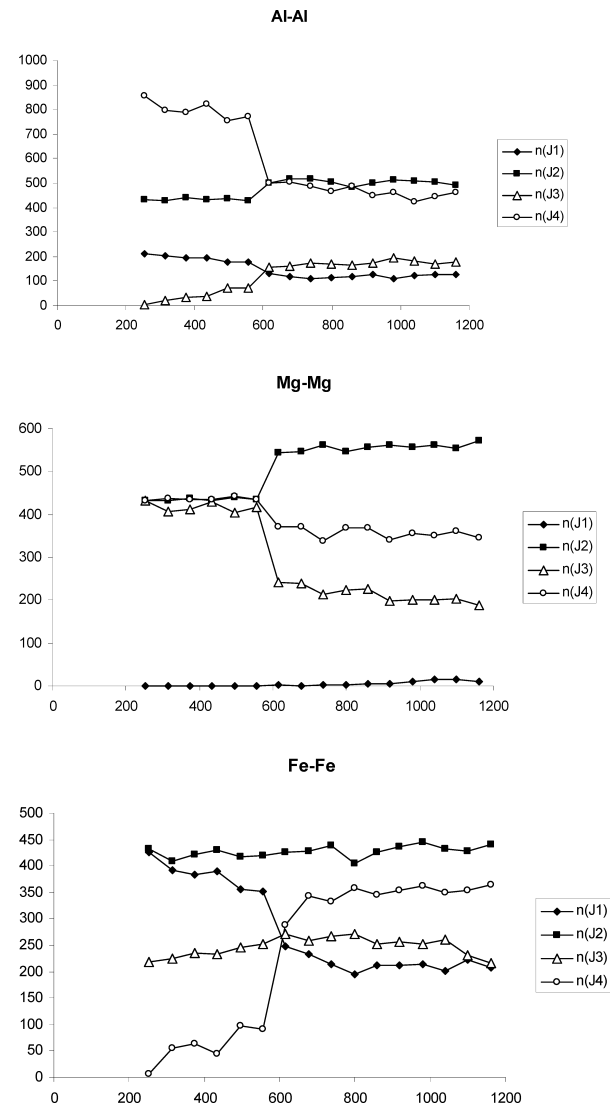

FIGURE 7. Plot of $n(J_{n,i-i})$ (i = Al, Fe, Mg) for Al/Fe/Mg = 1/1/1, showing order-disorder phase transition as discontinuities in certain $n(J_{n,i-i})$ values as a function of temperature.

smectites, and for this reason, we performed three sets of simulations, using the three different sets of J_n in Table 4 (cases 1, 2, and 3 described above). The results are shown in Figure 11. In these simulations, we do not observe long-range order, although short-range order is evident, with the Mg atoms attempting to disperse, and the Fe atoms showing some clustering. Accordingly, the form of the heat capacity anomaly in this system is different from the other three systems studied (Fig. 6).

One can observe subtle differences between the different simulations in Figure 11. For example, examining the partial ordering patterns for Fe, the simulation performed with J set 3 (Fig. 11c) shows evidence of Fe–Fe nearest-neighbor pairs and occasionally larger clusters of Fe, whilst these are less obvious in the simulations with J values from 1 (Fig. 11a) and 2 (Fig. 11b). Similarly, comparing the Al partial ordering patterns, we note that the simulation with J values from set 1 produces a

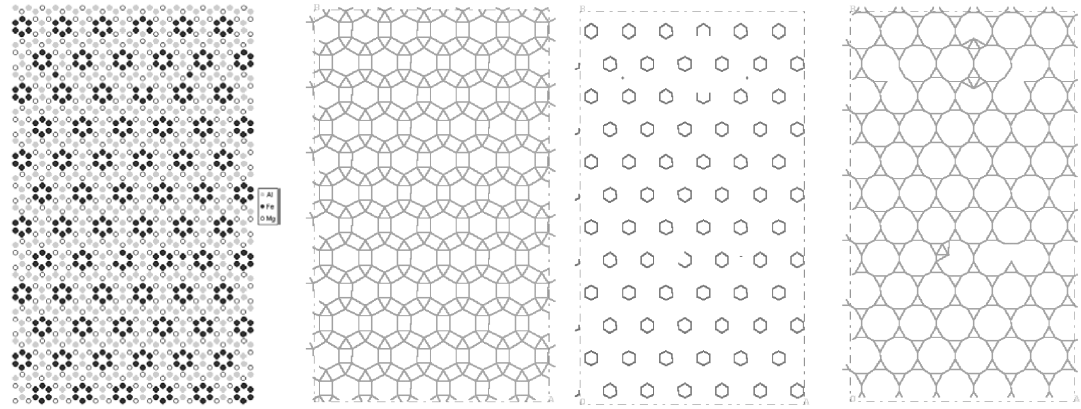

FIGURE 8. Low-temperature snapshot of the system Al/Fe/Mg = 1/1/1 (**a**). Black, grey, and white circles represent Fe, Al, and Mg, respectively. Partial ordering pattern is shown in graphs **b**, **c**, and **d** for Mg, Fe, and Al, respectively.

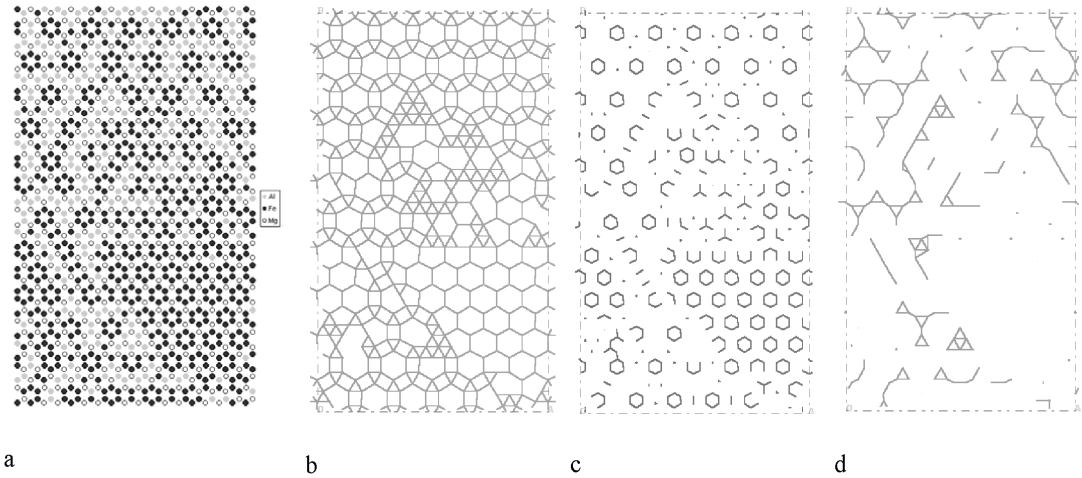

FIGURE 9. Low-temperature snapshot of the system Al/Fe/Mg = 1/3/2 (**a**), partial ordering patterns for Mg (**b**), Fe (**c**), and Al (**d**). Black, grey, and white circles represent Fe, Al, and Mg, respectively.

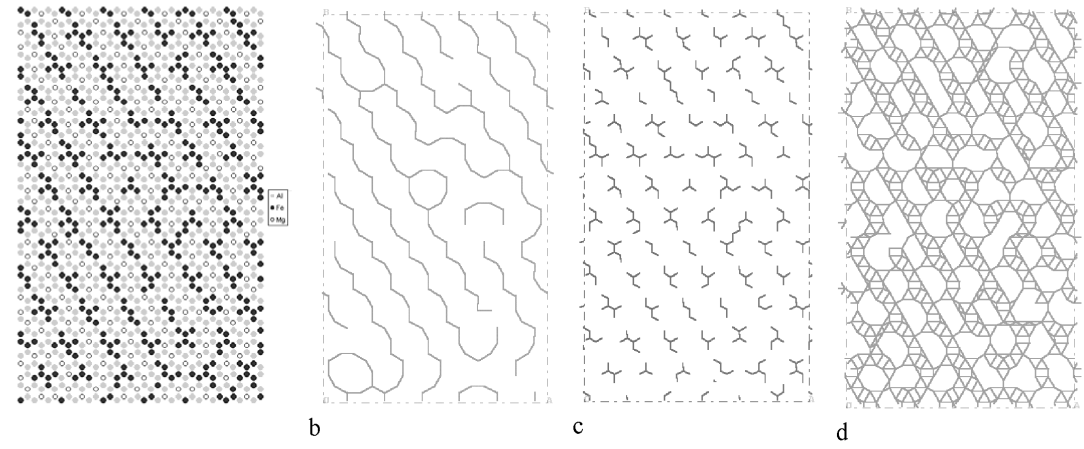

FIGURE 10. Model Al/Fe/Mg: 3/2/1. Low-temperature snapshot (**a**), partial ordering patterns for Mg (**b**), Fe (**c**), and Al (**d**). Black, grey, and white circles represent Fe, Al, and Mg, respectively.

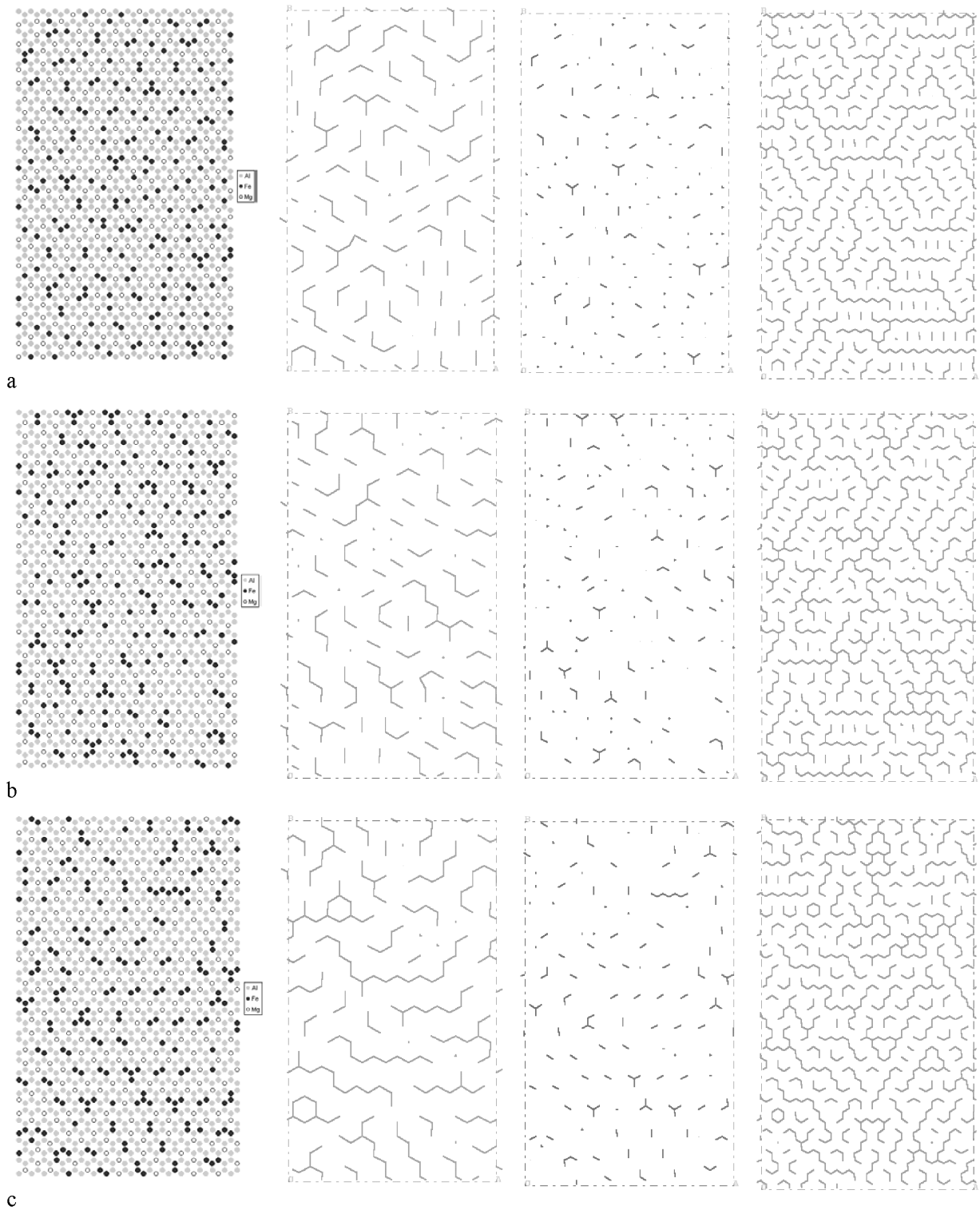

FIGURE 11. Low-temperature snapshots of the system Al/Fe/Mg = 4/1/1 for simulations performed with averaged J values (**a**), smectitic J_n (**b**), and illitic J_n (**c**). Partial ordering plots for each simulation are shown (left-right = Mg, Fe, Al). Black, grey, and white circles represent Fe, Al, and Mg, respectively.

pattern which is partially reproduced in the Al network in the simulation with *J* set 2, more so than in the simulation with *J* values from 3.

Systems 2 and 3 represent smectite and illite compositions, respectively. System 3 is for samples with higher tetrahedral and interlayer charge than those of model 2. In the lowest energy configuration of both systems, the Fe cations segregate forming small clusters of Fe, which are occasionally larger in the illite model (Fig. 11c). Previous experimental studies of clay minerals (Besson et al. 1987; Drits et al. 1997) found that the Fe distribution is not random and it tends to segregate from Al with a certain short-range ordering, but no clear description of this ordering was reported. RMC simulations based only on FTIR spectroscopic data of smectites and illites (Cuadros et al. 1999) found the existence of Fe clusters in both systems, with higher cluster sizes in illites. The IR data only gives short-range ordering information and the estimation of the clustering degree can only be approximate. Further RMC simulations based on FTIR and ^{27}Al-NMR data of these minerals (Sainz-Díaz et al. 2001c) corroborate the Fe clustering tendency but these clusters are very small and similar to those obtained in our MC simulations, where a slightly higher medium-range ordering of Fe^{3+} in illites relative to smectites was concluded (Fig. 12). Therefore, our MC simulations reproduce the cation distribution pattern of Fe^{3+} for illites and smectites found experimentally.

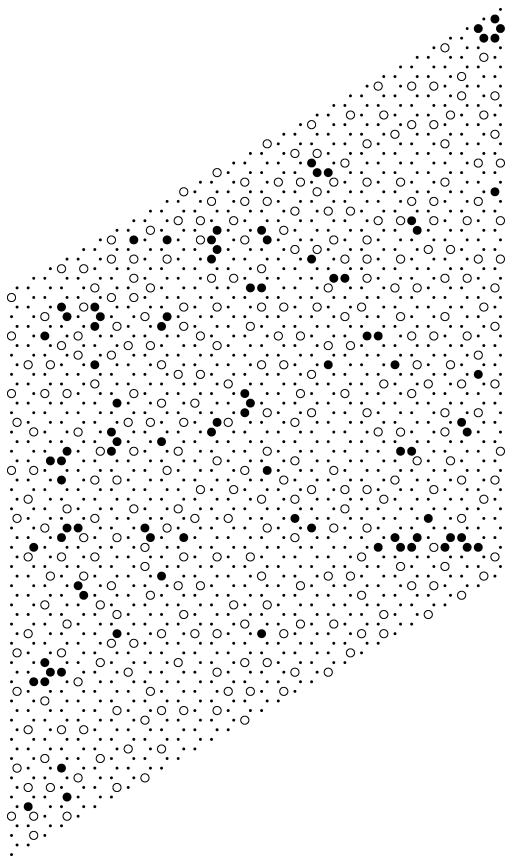

FIGURE 12. Cation distribution in the octahedral sheet for an illite/smectite sample (64% illite, octahedral composition = $Al_{3.13}Fe_{0.2}Mg_{0.67}$) obtained experimentally by means of FTIR, NMR, and RMC simulations (Sainz-Díaz et al. 2001c). Black circles, dots, and white circles represent Fe, Al, and Mg, respectively.

This work has shown how diverse and complex ordering behaviour can arise within simulations of three-species systems. In the systems studied here the diversity arises from changes in the relative proportions of the different species, and we believe it arises from the fact that the values of the exchange interactions for different pairs of species are significantly different. Of note is the formation of complex superstructure ordering in the Al/Fe/Mg 1/1/1 system, segregation into different ordered structures in the Al/Fe/Mg 1/3/2 system, ordering with many defects in the Al/Fe/Mg 3/2/1 system, and the formation of only short-range order in the Al/Fe/Mg 4/1/1 system.

The discrepancies on the cation ordering in the octahedral sheet of clay minerals found among experimental studies could be explained by the fact that the experiments take average values of the cation distribution in the different layers of the mineral that are not ordered each order. However, this ordering of octahedral cations is also highly dependant on the cation composition, as we conclude from our MC simulations.

The suite of samples investigated in this study was selected because of the correspondence of the samples to natural smectites and illites. The point that we believe we have demonstrated is that the agreement between the simulation results and experiments provides some validation for the methodology presented in the present work, and this approach can be applied for predictive proposes of cation ordering in clay minerals. The methodology presented in this paper can be very useful to study ordering phenomena in other solids, such as catalyzers, and semiconductors.

ACKNOWLEDGMENTS

The authors are grateful to J. Gale for permitting us to use the GULP program, to V. Botella for his fruitful discussions, and for the financial support of NERC (M.T. Dove), EPSRC (E.J. Palin), the Royal Society, and M.E.C. of Spain (C.I. Sainz-Díaz), and the PB97-1205 and BTE2000-1146-CO2-01 MCYT project and the Acciones Integradas UK/Spain joint research programme. The Monte Carlo simulations were performed on the University of Cambridge's High Performance Computing Facility and the Mineral Physics Group's Beowulf cluster.

REFERENCES CITED

Abbot, R.N., Jr., Post, J.E., and Burnham, C.W. (1989a) Treatment of the hydroxyl in structure-energy calculations. American Mineralogist, 74, 141–150.

Abbot, R.N., Jr., Burnham, C.W., and Post J.E. (1989b) Hydrogen in humite-group minerals: Structure-energy calculations. American Mineralogist, 74, 1300–1306.

Besson, G., Drits, V.A., Daynyak, L.G., and Smoliar, B.B. (1987) Analysis of cation distribution in dioctahedral micaceous minerals on the basis of IR spectroscopy data. Clay Minerals, 22, 465–478.

Bosenick, A., Dove, M.T., and Geiger, C.A. (2000) Simulation studies of pyrope-grossular solid solutions. Physics and Chemistry of Minerals, 27, 398–418.

Bosenick, A., Dove, M.T., Myers, E.R., Palin, E.J., Sainz-Díaz, C.I., Guiton, B., Warren, M.C., Craig, M.S., and Redfern, S.A.T. (2001) Computational methods for the study of energies of cation distributions: applications to cation-ordering phase transitions and solid solutions. Mineralogical Magazine, 65, 197–223.

Bush, T.S., Gale, J.D., Catlow, C.R.A., and Battle, P.D. (1994) Self-consistent interatomic potentials for the simulation of binary and ternary oxides. Journal of Materials Chemistry, 4, 831–837.

Collins, D.R. and Catlow, C.R.A. (1992) Computer simulations of structures and cohesive properties of micas. American Mineralogist, 77, 1172–1181.

Cuadros, J., Sainz-Díaz, C., Ramírez, R., and Hernández-Laguna, A. (1999) Analy-

sis of Fe segregation in the octahedral sheet of bentonitic illite-smectite by means of FT-IR, ^{27}Al MAS NMR and reverse Monte Carlo simulations. American Journal of Science, 299, 289–308.

Decarreau, A., Grauby, O., and Petit, S. (1992) The actual distribution of octahedral cations in 2:1 clay minerals: results from clay synthesis. Applied Clay Science, 7, 147–167.

Dove, M.T. and Heine, V. (1996) The use of Monte Carlo methods to determine the distribution of Al and Si cations in framework aluminosilicates from ^{29}Si MAS NMR data. American Mineralogist, 81, 349–362.

Dove, M.T., Thayaparam, S., Heine, V., and Hammonds, K.D. (1996). The phenomenon of low Al-Si ordering temperatures in aluminosilicates framework structures. American Mineralogist, 81, 349–362.

Drits, V.A., Dianyak, L.G., Muller, F., Besson, G., and Manceau, A. (1997) Isomorphous cation distribution in celadonites, glauconites and Fe-illites determined by infrared, Mössbauer and EXAFS spectroscopies. Clay Minerals, 32, 153–179.

Gale, J.D. (1997) GULP—a computer program for the symmetry adapted simulation of solids. Journal of the Chemical Society, Faraday Transactions, 93, 629.

Grauby, O., Petit, S., and Decarreau, A. (1991) Distribution of Al-Fe-Mg in octahedral sheets of synthetic smectites : Study of three binary solid-solutions. Proceedings of the 7th EUROCLAY Conference, 441–446.

Herrero, C.P. and Sanz, J. (1991) Short-range order of the Si,Al distribution in layer silicates, Journal of Physics and Chemistry of Solids, 52, 1129–1135.

Jackson, R.A. and Catlow, C.R.A. (1988) Computer simulation studies on zeolite structures. Molecular Simulation, 1, 207–224.

Lear, P.R. and Stucki, J.W. (1990) Magnetic properties and site occupancy of iron in nontronite. Clay Minerals, 25, 3–14.

Manceau, A., Lanson, B., Drits, V.A., Chateigner, D., Gates, W.P., Wu, J., Huo, D., and Stucki, J.W. (2000) Oxidation-reduction mechanism of iron in dioctahedral smectites: I. Crystal chemistry of oxidized reference nontronites. American Mineralogist, 85, 133–152.

Morris, H.D., Bank, S., and Ellis, P.D. (1990) ^{27}Al NMR spectroscopy of iron-bearing montmorillonite clays. Journal of Physical Chemistry, 94, 3121–3129.

Muller, F., Besson, G., Manceau, A., and Drits, V.A. (1997) Distribution of isomorphous cations within octahedral sheets in montmorillonite from Camp-Bertaux. Physics and Chemistry of Minerals, 24, 159–166.

Palin, E.J., Dove, M.T., Redfern, S.A.T., Bosenick, A., Sainz-Díaz, C.I., and Warren, M.C. (2001) Computational study of tetrahedral Al-Si ordering in muscovite. Physics and Chemistry of Minerals, 28, 534–544.

Post, J.E. and Burnham, C.W. (1986) Ionic modeling of mineral structures and energies in the electron gas approximation: TiO_2 polymorphs, quartz, forsterite, diopside. American Mineralogist, 71, 142–150.

Sainz-Díaz, C.I., Hernández-Laguna, A., and Dove, M.T. (2001a) Modelling of dioctahedral 2:1 phyllosilicates by means of transferable empirical potentials. Physics and Chemistry of Minerals, 28, 130–141.

Sainz-Díaz, C.I., Hernández-Laguna, A., and Dove, M.T. (2001b) Theoretical modelling of cis-vacant and trans-vacant configurations in the octahedral sheet of illites and smectites. Physics and Chemistry of Minerals, 28, 322–331.

Sainz-Díaz, C.I., Cuadros, J., and Hernández-Laguna, A. (2001c) Cation distribution in the octahedral sheet of dioctahedral 2:1 phyllosilicates by using inverse Monte Carlo methods. Physics and Chemistry of Minerals, 28, 445–454.

Sainz-Díaz, C.I., Palin, E.J., Hernández-Laguna, A., Dove, M.T. (2003) Octahedral cation ordering of dioctahedral 2:1 phyllosilicates by means of Monte Carlo simulations. Physics Chemical Minerals (in press).

Schröder, K.-P., Sauer, J., Leslie, M., Catlow, C.R.A., and Thomas, J.M. (1992) Bridging hydroxyl groups in zeolitic catalysts: a computer simulation of their structure, vibrational properties and acidity in protonated faujasites (H-Y zeolites). Chemical Physics Letters, 188, 320–325.

Schroeder, P.A. (1993) A chemical, XRD, and ^{27}Al MAS NMR investigation of Miocene Gulf Coast shales with application to understanding illite-smectite crystal-chemistry. Clays Clay Minerals, 41, 668–679.

Thayaparam, S., Heine, V., Dove, M.T., and Hammonds, K.D. (1996) A computational study of Al/Si ordering in cordierite. Physics and Chemistry of Minerals, 23, 127–139.

Tsipursky, S.I. and Drits, V.A. (1984) The distribution of octahedral cations in the 2:1 layers of dioctahedral smectites studied by oblique-texture electron diffraction. Clay Minerals, 19, 177–193.

Warren, M.C., Dove, M.T., Myers, E.R., Bosenick, A., Palin, E.J., Sainz-Díaz, C.I., Guiton, B., and Redfern, S.A.T. (2001) Monte Carlo methods for the study of cation ordering in minerals. Mineralogical Magazine, 65, 225–252.

Winkler, B., Dove, M.T., and Leslie, M. (1991) Static lattice energy minimization and lattice dynamics calculations on aluminosilicate minerals. American Mineralogist, 76, 313–331.

MANUSCRIPT RECEIVED AUGUST 27, 2002
MANUSCRIPT ACCEPTED DECEMBER 23, 2002
MANUSCRIPT HANDLED BY JAMES KUBICKI